Optimal quantum metrology of two-photon absorption

IOP Publishing Quantum Sci. Technol. 9 (2024) 035042 https://doi.org/10.1088/2058-9565/ad466b

Quantum Science and Technology

OPEN ACCESS

RECEIVED
21 November 2023

REVISED
24 March 2024

ACCEPTED FOR PUBLICATION
2 May 2024

PUBLISHED
29 May 2024

PAPER

Optimal quantum metrology of two-photon absorption

Athena Karsa[1,2,*], **Ranjith Nair**[3], **Andy Chia**[4], **Kwang-Geol Lee**[5] **and Changhyoup Lee**[2,*]

[1] School of Physics & Astronomy, University College London, London WC1E 6BT, United Kingdom
[2] Korea Research Institute of Standards and Science, Daejeon 34113, Republic of Korea
[3] School of Physical and Mathematical Sciences, Nanyang Technological University, 639763, Singapore
[4] Centre for Quantum Technologies, National University of Singapore, 117543, Singapore
[5] Department of Physics, Hanyang University, Seoul 04763, Republic of Korea
[*] Authors to whom any correspondence should be addressed.

E-mail: athena.karsa@gmail.com and changhyoup.lee@gmail.com

Keywords: quantum metrology, two-photon absorption, optimisation, quantum Fisher information

Abstract

Two-photon absorption (TPA) is a nonlinear optical process with wide-ranging applications from spectroscopy to super-resolution imaging. Despite this, the precise measurement and characterisation of TPA parameters are challenging due to their inherently weak nature. We study the potential of single-mode quantum light to enhance TPA parameter estimation through the quantum Fisher information (QFI). Discrete variable quantum states (defined to be a finite superposition of Fock states) are optimised to maximise the QFI for given absorption, revealing a quantum advantage compared to both the coherent state (classical) benchmark and the single-mode squeezed vacuum state. For fixed average energy $\bar{n} \in 2\mathbb{N}$, the Fock state is shown to be optimal for large TPA parameters, while a superposition of vacuum and a particular Fock state is optimal for small absorption for all $\bar{n}$. This differs from single-photon absorption where the Fock state is always optimal. Notably, photon counting is demonstrated to offer optimal or nearly optimal performance compared to the QFI bound for all levels of TPA parameters for the optimised quantum probes, and their quantum advantage is shown to be robust to single-photon loss. Our findings provide insight into known limiting behaviours of Gaussian probes and their different FI scalings under photon counting ($\propto \bar{n}^2$ for squeezed vacuum states versus $\bar{n}^3$ for coherent states). The squeezed state outperforms coherent states for small TPA parameters but underperforms in the intermediate regime, becoming comparable in the large absorption limit. This can be explained through fundamental differences between behaviours of even and odd number Fock states: the former's QFI diverges in both large and small absorption limits, while the latter diverges only in the small absorption limit, dominating at intermediate scales.

1. Introduction

The study and use of nonclassical states of light is ubiquitous in quantum technologies, providing a potential resource for achieving a quantum enhancement in tasks such as metrology [1, 2], imaging [3] and spectroscopy [4]. Of particular interest is their possible role within nonlinear light-matter interactions such as two-photon absorption (TPA), the subject of this work. Notably, the TPA probability for a squeezed light source scales linearly with the intensity of the light field, as opposed to the quadratic scaling observed with laser light [5–10]. This effect may potentially enable nonlinear spectroscopy and microscopy at low photon fluxes which could in turn permit TPA-based protocols to interrogate photosensitive samples, or even living organisms, while mitigating their degradation [11–16], for example, by enabling infrared imaging which bypasses tissue.

Recent years have seen a multitude of ongoing developments in quantum-enhanced optical sensing protocols, owing to theoretical and experimental progress providing access to new quantum sources and means for their use [17, 18]. Concerning quantum-enhanced absorption measurements, the regime of single-photon absorption was naturally explored first [19, 20]. The Fock state at any fixed photon number

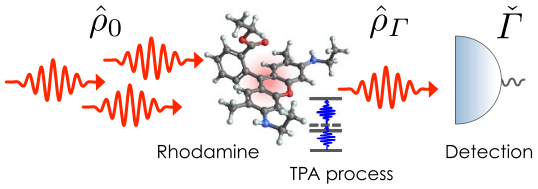

Figure 1. Schematic diagram of two-photon absorption (TPA) measurement. An input quantum state of light $\hat{\rho}_0$ illuminates a medium comprising TPA molecules (e.g. rhodamine) for a time t which induce an incoherent TPA process with interaction strength conveniently captured by the dimensionless parameter $\Gamma = 1 - \exp(-\gamma t)$, where γ is the TPA rate, taking values in $[0, 1)$ (cf equation (12)). After the interaction, the resultant output state $\hat{\rho}_\Gamma$ is measured by a detector, followed by post-processing to generate an estimate $\check{\Gamma}$.

(PN) ($\bar{n}$) was shown to saturate the ultimate bound of precision (maximised over all single-mode probes with average PN $\bar{n}$) given by $1/4\bar{n}$ for a single run [21, 22], independent of the amount of absorption.

More recently, interest has been targeted towards TPA with focus primarily on the quantum metrological properties of Gaussian states [23, 24]. Their expression in terms of a unitary operation acting on the vacuum allows for a simplification of the TPA analysis that, however, is valid only in the regime of extremely low TPA rates. While it is possible to consider this regime a useful one, since typical TPA cross-sections are generally small (often $\lesssim 0.1$ [25–27]), this approach fails to allow for the study of arbitrary quantum states and a global comparison of their metrological potential across all possible scales of absorption.

This work studies the metrological power of various bosonic single-mode states $\hat{\rho}_0$ for estimating TPA rates as modelled by (illustrated in figure 1),

$$\frac{\mathrm{d}}{\mathrm{d}t}\hat{\rho}_t = \gamma \mathscr{L}\hat{\rho}_t \,, \tag{1}$$

where γ is the TPA rate to be estimated, and $\mathscr{L}$ is a superoperator in the Lindblad form, defined for any $\hat{J}$ and $\hat{s}$ by [28]

$$\mathscr{L}\hat{s} \equiv \hat{J}\hat{s}\hat{J}^\dagger - \frac{1}{2}\hat{J}^\dagger\hat{J}\hat{s} - \frac{1}{2}\hat{s}\hat{J}^\dagger\hat{J} \,. \tag{2}$$

For TPA, we take $\hat{J} = \hat{a}^2/\sqrt{2}$ with $\hat{a}$ being the bosonic annihilation operator. We have set $\hbar = 1$ and moved into a rotating frame in which the the free harmonic evolution of the probe field appears stationary.

Our primary aim is to find, for a fixed average PN $\bar{n}$, the probe state $\hat{\rho}_0$ which maximises the quantum Fisher information (QFI) associated with estimating γ. Indeed, the QFI places—via the quantum Cramér–Rao (QCR) inequality (see section 2.1)—a lower bound on the mean squared error of estimating the TPA rate γ. Since this bound is independent of the actual quantum measurement performed, it constitutes a fundamental limit to the estimation accuracy.

We find that Fock states with $\bar{n} \in 2\mathbb{N}$ are optimal only in the limit of very large TPA, with competing behaviour between squeezed vacuum and coherent states at the low to intermediate TPA scales. This suggests an absorption-dependent behaviour in the form of the optimal probe. With this in mind, we optimise a general discrete variable (DV) quantum state of the form

$$|\psi_{\mathrm{DV}}\rangle = \sum_{j=0}^{N_{\max}} c_j |j\rangle \,, \tag{3}$$

to maximise the QFI given a fixed TPA parameter value, where $|j\rangle$ is a Fock state with PN j. The theoretically optimal single-mode quantum probe is found and our analysis also provides insight into the observed behaviours of the coherent, squeezed vacuum and Fock states, to which our probe is compared. While the Fock state is not always optimal, superpositions of the vacuum with another Fock state are, where the PN of the latter state is a function of the TPA parameter.

Further, we show that the QFI of the optimal DV states can almost always be fully harnessed by ideal (quantum efficiency $\xi = 1$) photon counting measurements. We also consider inefficient photon counting and show that the QFI of the optimal DV states degrades gracefully with decreasing ξ and can still beat the performance of coherent and squeezed vacuum probes of the same energy.

2. Background

Aspects of parameter estimation theory are briefly reviewed here. We also discuss the TPA model, including its assumptions and the computations that lead to the results of section 3.

2.1. Quantum parameter estimation theory

The goal of parameter estimation is to determine the value of some unknown parameter ε (which we take to be deterministic) given a set of observed data, say $\boldsymbol{y} \equiv (y_1, y_2, \ldots, y_\nu)$ (which we assume to be discrete). The data $\boldsymbol{y}$ are outcomes of measurements drawn from the conditional probability $p(\boldsymbol{y}|\varepsilon)$, conditioned on the true value of ε. An estimator $\check{\varepsilon}(\boldsymbol{y})$ is then constructed from $\boldsymbol{y}$ to form an inference of ε. For an unbiased estimator, i.e. one for which $\langle\check{\varepsilon}\rangle = \varepsilon$, classical estimation theory bounds the mean-squared error of $\check{\varepsilon}$ by the CR inequality

$$\langle(\check{\varepsilon} - \varepsilon)^2\rangle \geqslant \frac{1}{\nu\mathcal{F}}\,, \tag{4}$$

where $\langle g(\boldsymbol{y})\rangle = \sum_{\boldsymbol{y}} p(\boldsymbol{y}|\varepsilon)\, g(\boldsymbol{y})$ for any $g(\boldsymbol{y})$. The bound is determined by the FI, defined as

$$\mathcal{F} = \sum_{\boldsymbol{y}} p(\boldsymbol{y}|\varepsilon) \left[\frac{\partial}{\partial\varepsilon} \ln p(\boldsymbol{y}|\varepsilon)\right]^2 . \tag{5}$$

Quantum parameter estimation theory is necessary when the measurement yielding $\boldsymbol{y}$ becomes a quantum process, which is described by a positive operator-valued measure,

$$\mathbb{P} = \left\{ \hat{\Pi}_{\boldsymbol{y}} \,\middle|\, \hat{\Pi}_{\boldsymbol{y}} \geqslant 0, \sum_{\boldsymbol{y}} \hat{\Pi}_{\boldsymbol{y}} = \hat{\mathbb{1}} \right\} . \tag{6}$$

The FI retains its form as in equation (5), but the probability of observing $\boldsymbol{y}$ is now given by $p(\boldsymbol{y}|\varepsilon) = \mathrm{Tr}\big[\hat{\rho}_\varepsilon \hat{\Pi}_{\boldsymbol{y}}\big]$, where $\hat{\rho}_\varepsilon$ is the state of the system carrying ε. A further reduction of the CR bound is then possible, expressed by the well-known QCR inequality [29],

$$\frac{1}{\mathcal{F}} \geqslant \frac{1}{\mathcal{F}_{\mathrm{Q}}}\,. \tag{7}$$

The quantity $\mathcal{F}_{\mathrm{Q}}$ is the QFI, defined by

$$\mathcal{F}_{\mathrm{Q}} = \mathrm{Tr}\left[\hat{\rho}_\varepsilon \hat{L}_\varepsilon^2\right] , \tag{8}$$

where $\hat{L}_\varepsilon$ is the symmetric logarithmic derivative (SLD), defined as a Hermitian solution to

$$\frac{\mathrm{d}\hat{\rho}_\varepsilon}{\mathrm{d}\varepsilon} = \frac{1}{2}\left(\hat{L}_\varepsilon\hat{\rho}_\varepsilon + \hat{\rho}_\varepsilon\hat{L}_\varepsilon\right) . \tag{9}$$

It is straightforward to show from equation (9) that

$$\hat{L}_\varepsilon = 2\sum_{\substack{k \\ (\lambda_k+\lambda_l>0)}}\sum_{l} \frac{\langle\lambda_l|\left(\mathrm{d}\hat{\rho}_\varepsilon/\mathrm{d}\varepsilon\right)|\lambda_k\rangle}{\lambda_k+\lambda_l} |\lambda_l\rangle\langle\lambda_k| , \tag{10}$$

where $\hat{\rho}_\varepsilon|\lambda_k\rangle = \lambda_k|\lambda_k\rangle$, and note that λ_k and $|\lambda_k\rangle$ are ε-dependent. The QFI in equation (8) arises as a maximisation of the FI in equation (5) over all possible measurements. That is, $\mathcal{F}_{\mathrm{Q}} = \max_{\mathbb{P}}\mathcal{F}$, and the optimal $\mathbb{P}$ can be constructed over the eigenbasis of $\hat{L}_\varepsilon$ [30].

2.2. TPA model and computations

It is convenient to nondimensionalise equation (1) by using the dimensionless parameter $\varepsilon = \gamma\, t$. Our model for TPA then becomes

$$\frac{\mathrm{d}}{\mathrm{d}\varepsilon}\hat{\rho}_\varepsilon = \mathscr{L}\,\hat{\rho}_\varepsilon\,. \tag{11}$$

This reparametrisation also makes sense physically because the total number of TPA events in a given sample can be achieved by controlling how much time the probe light interacts with the sample. Note that we have assumed the molecules or atoms of the TPA sample to be in their ground state. This ensures the only possible

two-photon transitions in the sample are absorption processes, i.e. no two-photon emissions occur. Two-photon emission from sample molecules may be accounted for by another Lindblad superoperator with $\hat{J} = \hat{a}^{\dagger 2}/\sqrt{2}$, which lead to other nontrivial effects [31–33]. As in [23], one-photon transitions in the TPA sample are neglected.

The exact analytical solution $\hat{\rho}_\varepsilon$ of equation (11) for an arbitrary input state $\hat{\rho}_0$ has been obtained in the literature [34–38]. However, the exact solution from the literature is rather complicated and we resort to numerical computations of the QFI. Even so, the arbitrariness of $\hat{\rho}_0$ permitted by the exact solution is still important, as it affords us a way to find states $\hat{\rho}_0$ that maximise the QFI. The exact solution is explained in appendix A. To calculate the QFI we need to calculate first the SLD as defined in equation (10), which in turns requires λ_k and $|\lambda_k\rangle$. For each value of ε, the output state $\hat{\rho}_\varepsilon$ is numerically evaluated using equation (A6) from appendix A, and then diagonalised to find λ_k and $|\lambda_k\rangle$. This then allows us to evaluate $\langle\lambda_l|\left(\mathrm{d}\hat{\rho}_\varepsilon/\mathrm{d}\varepsilon\right)|\lambda_k\rangle$ using equations (2) and (11) with $\hat{J} = \hat{a}^2/\sqrt{2}$. The SLD is then constructed according to equations (2) and (10), from which the QFI can be readily calculated using equation (8).

While we carry out our calculations with the variable ε, it is more convenient to consider the final results (such as the QFI) in terms of

$$\Gamma = 1 - \mathrm{e}^{-\varepsilon}\,. \tag{12}$$

This is because ε is unbounded, taking on values in $[0,\infty)$, whereas Γ has values restricted to $[0,1)$. The finite range of Γ is helpful for plotting and visualisation. Note that ε is in one-to-one correspondence with Γ. If ε increases (or decreases), Γ increases (or decreases). Thus no ambiguity arises in using Γ to discuss our results[6].

3. Results and discussion

3.1. TPA parameter estimation under an energy constraint

3.1.1. Fock states

In the case of single-photon absorption estimation, with Lindblad operator $\hat{J} = \hat{a}$, Fock states at any fixed PN are known to unconditionally saturate the ultimate bound on precision [20, 21]. In the case of TPA parameter estimation, on the other hand, this does not hold for all values of mean PNs and TPA parameters. In particular, there exists a dramatic difference in the behaviours of even and odd Fock states subject to TPA evolution, and their resultant precision to TPA parameter estimation. This contrast is illustrated in figure 2. For weak TPA, Fock states $|n\rangle$ with higher n have higher QFIs, all diverging as $\Gamma \to 0$. In this limit, the scaling of the QFI for a Fock state with PN $\bar{n}$ goes as (see appendix C for the derivation),

$$\mathcal{F}_{\mathrm{Q,F}} \simeq \frac{\bar{n}\,(\bar{n}-1)}{2\Gamma}\,. \tag{13}$$

In the limit of strong TPA, QFIs for odd Fock states decay to zero while those for even Fock states diverge once again. The performances of Fock states with $\bar{n} = 2$ and $\bar{n} = 3$ will be compared with other single-mode probe states of the same mean energy in the next section.

3.1.2. Optimal DV, squeezed vacuum and coherent states

Since the QFI depends only on the input state $\hat{\rho}_0$, it can be maximised when the input state is chosen appropriately. In this subsection, we maximise the QFI over a large class of input states subject to the global constraint of fixed mean PN $\bar{n}$.

An optimisation is performed over all possible DV quantum states which take the form of equation (3) for a given maximum occupation number $N_{\max}$, and a fixed mean PN $\bar{n}$. For simplicity, the coefficients c_j are assumed to be real, and we set $N_{\max} = 10$. A nested optimisation procedure is employed, comprising two successive algorithms: the evolutionary algorithm library EvoTorch [39] is used for a coarse-grained global search of maxima, and then its output forms the seed of a subsequent adaptive moment estimation optimiser (called Adam) which fine-tunes the result through gradient descent. This procedure is carried out for each value of Γ, yielding paired results comprising the maximal QFI and the optimal DV quantum state attaining that QFI.

The QFI corresponding to different optimal DV states are compared with those for squeezed vacuum states $|\xi\rangle = \hat{S}(\xi)|0\rangle$ with a squeezing operator $\hat{S}(\xi) = \exp\left[(\xi^*\hat{a}^2 - \xi\,\hat{a}^{\dagger 2})/2\right]$, where $\xi = r\exp(\mathrm{i}\theta_\mathrm{s})$ and $r \geqslant 0$; Fock states $|n\rangle$; and coherent states $|\alpha\rangle = \hat{D}(\alpha)|0\rangle$ with a displacement operator $\hat{D}(\alpha) = \exp\left(\alpha\hat{a}^\dagger - \alpha^*\hat{a}\right)$ for

[6] We do not recast equation (1) in terms of $\Gamma = 1 - \exp(-\gamma t)$ at the outset because this results in an explicitly Γ-dependent equation. The solution to such an equation then becomes very difficult to evaluate.

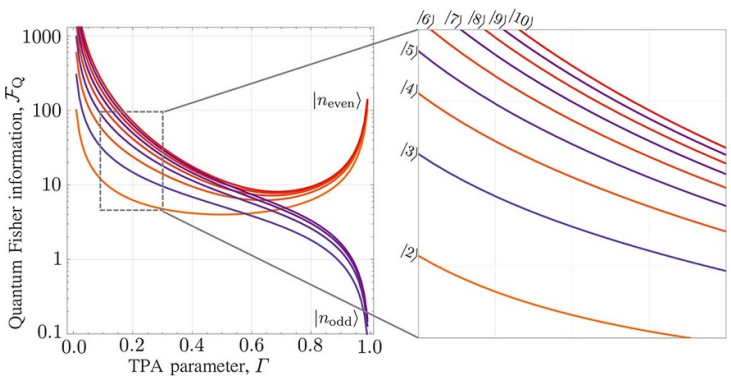

Figure 2. QFI for TPA parameter estimation for even and odd Fock states where $n_{\text{even}} = 0, 2, 4, \ldots$, and $n_{\text{odd}} = 1, 3, 5, \ldots$. Clearly shown are differing behaviours across Γ, which will explain the behaviours of the other probe states to be considered in this work.

$\alpha = |\alpha| \exp(\mathrm{i}\theta_{\mathrm{d}})$. The coherent state serves as a classical benchmark allowing us to assess the quantum advantage in using $|\xi\rangle$, $|n\rangle$, or $|\psi_{\text{DV}}\rangle$ as probe states. For fair comparisons, a fixed mean PN $\bar{n}$ is enforced by setting $\bar{n} = n = \sinh^2(r) = |\alpha|^2$. We also set $\theta_{\mathrm{s}} = \theta_{\mathrm{d}} = 0$ for simplicity. This is permitted since the QFI is actually independent of these phases (see appendix E).

The QFIs resulting from the optimisation are depicted as a function of Γ in figures 3(a) and (b) for mean PNs $\bar{n} = 2$ and 3, respectively. The QFIs for optimal DV states are dominant across the entire range of Γ while the squeezed vacuum, Fock, and coherent states exhibit competitive behavior between themselves. For $\bar{n} = 2$, the squeezed vacuum state surpasses the other two states for small Γ, but the Fock state, i.e. $|2\rangle$, starts to be dominant when $\Gamma \gtrsim 0.2$ and coincides with the optimal DV states when $\Gamma \gtrsim 0.45$. While the Fock state provides a quantum advantage over the coherent state across all Γ values, the squeezed vacuum state's quantum advantage only exists at small or large Γ. The QFIs of all considered states diverge as $\Gamma \to 0$ or $\Gamma \to 1$, except for the coherent state whose QFI approaches a finite value of $\bar{n}^3 + \bar{n}^2/2$ as $\Gamma \to 0$ (note that this value holds for all $\bar{n} \in \mathbb{R}$). For $\bar{n} = 3$, the overall behaviours are similar to the case of $\bar{n} = 2$, except now the Fock state, i.e. $|3\rangle$, has a monotonically decreasing QFI as Γ increases (which was also seen in figure 2).

Figures 3(c) and (d) illustrate the populations $\{|c_j|^2\}_{j=0}^{N_{\max}}$ of the optimal DV states, with maximum occupation number $N_{\max} = 10$, which resulted in the maximised QFIs of figures 3(a) and (b). For $\bar{n} = 2$, we can see that the resultant optimal DV state can be written in the simple form of the weighted ON state $|\text{ON}\rangle = c_0|0\rangle + c_N|N(\Gamma)\rangle$, where $N(\Gamma)$ denotes the optimal occupation found through optimisation for a given Γ, and the weights c_0, c_N take values to yield the mean $\bar{n}$: $c_0 = \sqrt{1 - c_N^2}$ and $c_N = \sqrt{\bar{n}/N(\Gamma)}$.

Following an equivalent procedure as for the pure Fock state but taking into account the weighting c_N when Γ is small, it can be determined that as $\Gamma \to 0$, the QFI of this optimal probe is

$$\mathcal{F}_{\text{Q,ON}} \simeq \frac{\bar{n}(N-1)}{2\Gamma}. \tag{14}$$

In the case of $\bar{n} = 3$, the optimal DV state can be written similarly in the form of the weighted ON state, but it evolves into a superposition of $|2\rangle$ and $|4\rangle$ when $\Gamma \gtrsim 0.45$. Across this region it can be found that there exists a wide range of states with similar QFIs, leading to multiple local optima and some transient points in figure 3(d).

The differing behaviours across Γ for even and odd Fock states manifests in the way the value of $N(\Gamma)$ of the optimal probe, in the form of ON state, varies across Γ as well. In particular, it is apparent that there exists, for some value of Γ, a phase transition between odd and even number state dominance in terms of their associated QFIs. This is discussed further in appendix D.

The form of the optimal probe also provides further insight into the already known behaviours for coherent and squeezed vacuum states in the limit of $\Gamma \to 0$. In this regime, both the coherent state QFI and photon-counting FI saturates at $\bar{n}^3 + \bar{n}^2/2$ while the squeezed vacuum state's FI is $\sim 10\bar{n}^2$ [23]. For relatively low energies, $\bar{n} \lesssim 10$, the squeezed vacuum can obtain higher precision than the coherent state even with sub-optimal photon counting. At these energies, however, the heavy-tailed distribution of the squeezed vacuum state naturally emulates our proposed optimal probe, with a larger proportion of its population in higher-energy states, while the coherent state remains narrowly distributed around its mean, i.e. smaller populations in higher-energy states. As the mean energy is progressively increased, the optimal probe becomes closer in distribution to the pure Fock state which the coherent state's PN distribution more closely resembles, allowing it to outperform the squeezed vacuum.

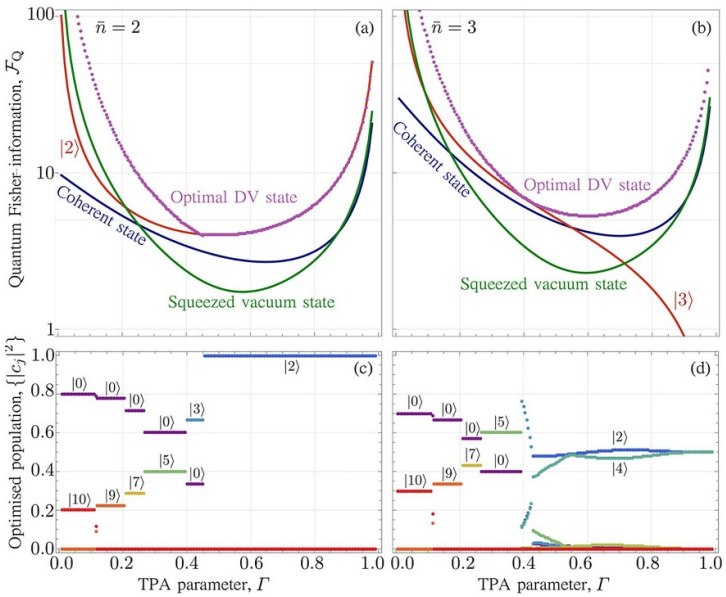

Figure 3. (a) and (b) QFI as a function of Γ of the optimal DV probe state with $N_{\max} = 10$, compared with that of the coherent, squeezed vacuum and pure Fock state for a mean number of photons $\bar{n} = 2$ and 3, respectively. (c) and (d) The corresponding optimised DV state populations $\{|c_j|^2\}$, yielding optimised DV probe $|\psi_{\text{DV}}\rangle = \sum_{j=0}^{N_{\max}} c_j |j\rangle$ attaining the maximum QFI for TPA parameter estimation, across all Γ. Note that for each value of Γ, all values of $\{|c_j|^2\}$ with $j = 0, \ldots, 10$ are plotted and coloured according to the rainbow across the range. For most data sets, all coefficients are zero except those corresponding to the vacuum and the optimal $|N\rangle$ for the Γ in question.

This explanation can go further to also explain behaviours seen outside the limit of vanishing Γ: intermediate to high TPA parameters show the optimal probe comprising of Fock states becomes increasingly centered around its mean (with optimised $N \to \bar{n}$) with QFI contributions from odd number states becoming dominant; here the coherent state yields higher precision than the squeezed vacuum. Eventually, with the degradation of all odd number state contributions to zero and the divergence of even number state contributions, we see the squeezed vacuum's QFI recovering once again as $\Gamma \to 1$.

Note that the results of the optimisation, depicted in figure 3, are ultimately constrained by imposing $N_{\max} = 10$. However, this is only in the regions where $\Gamma \lesssim 0.1$. Increasing the maximum occupation number would, in this region, yield optimal probes with progressively increasing odd number state contributions as $\Gamma \to 0$, ending with that corresponding to $N_{\max}$, with associated QFIs following equation (14) in this limit. The remainder of the results for $\Gamma \gtrsim 0.1$ would remain unchanged. Of course, any benefit of increasing $N_{\max}$ in this region is still subject to practical considerations.

Note also that it is possible that allowing all c_j to take complex values would yield still better performing probes. Nevertheless, our results show that even within the restricted landscape of values considered, one can achieve vast improvements in sensitivities for TPA rate estimation compared to the Gaussian probe states studied hitherto.

3.2. Quantum advantage

Figure 4 shows the quantum advantage in TPA parameter estimation afforded by the use of the three quantum states relative to the coherent state benchmark: the squeezed vacuum, Fock, and optimal DV probe. The quantum advantage is defined as

$$\text{QA} = \frac{\mathcal{F}_{\text{Q},\square} - \mathcal{F}_{\text{Q,Coh}}}{\mathcal{F}_{\text{Q,Coh}}}, \tag{15}$$

where $\mathcal{F}_{\text{Q},\square}$ is the QFI for the specific quantum state where we take $\square \in \{\text{SV}, \text{F}, \text{opt}\}$, denoting the squeezed vacuum, Fock and optimal DV probe, respectively.

For $\bar{n} = 2$, the optimal DV probe and Fock state always show a quantum advantage while there is a region of intermediate Γ where the squeezed vacuum probe loses its advantage. When $\bar{n} = 3$, again the optimal DV probe consistently shows a quantum advantage while the Fock state eventually loses it in the limit of large Γ. The squeezed vacuum state, like before, has a quantum advantage for small Γ, losing it for intermediate absorption values before regaining it as $\Gamma \to 1$.

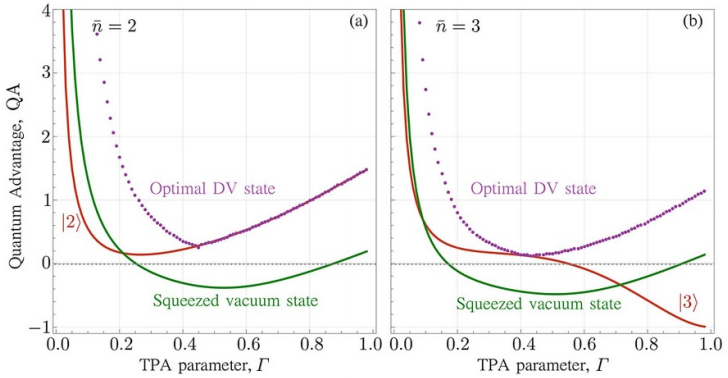

Figure 4. Quantum advantage, QA, of the squeezed vacuum, Fock and optimal DV state for TPA parameter estimation relative to the coherent state classical benchmark, quantified via their QFIs, for (a) $\bar{n} = 2$, and (b) $\bar{n} = 3$.

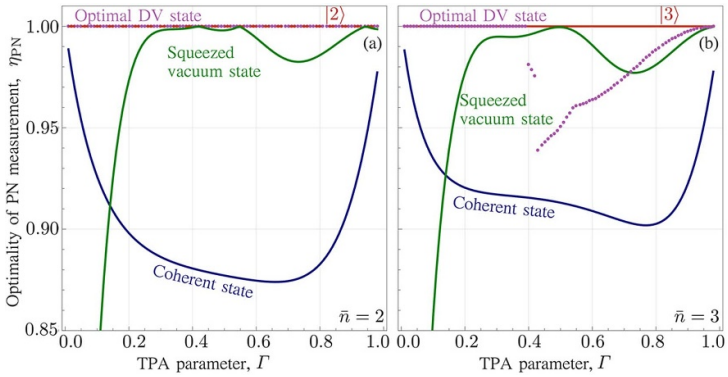

Figure 5. Efficiency of photon number (PN) measurements, η_{PN} for the squeezed vacuum, Fock, optimal DV and coherent state for TPA parameter estimation when (a) $\bar{n} = 2$, and (b) $\bar{n} = 3$.

3.3. PN detection

To show how good PN measurements are for TPA parameter estimation using each of the quantum states considered in this work, we define the efficiency of photon counting as the following ratio

$$\eta_{\mathrm{PN}} = \frac{\mathcal{F}_{\mathrm{PN}}}{\mathcal{F}_{\mathrm{Q}}}, \tag{16}$$

where $\mathcal{F}_{\mathrm{PN}}$ is the FI due to PN measurements. The results are plotted in figure 5.

For coherent states, photon counting is never completely optimal but improves in the limits of $\Gamma \to 0$ and $\Gamma \to 1$. In comparison, for a squeezed vacuum probe, photon counting is far from optimal when absorption is small and, overall, improves to becoming nearly optimal for increasing TPA. Meanwhile Fock state QFIs are, unsurprisingly, saturated by photon counting.

Remarkably, when the optimal probe is of the form of the ON state, the optimal measurement that saturates the QFI is simple photon counting. There are, however, some subtle intricacies to this fact depending on the nature of N: photon-counting is always the optimal measurement for ON states with $N = N_{\mathrm{o}} \in \mathbb{O}$, where $\mathbb{O}$ refers to the set of odd positive integers, while, for ON states with $N = N_{\mathrm{e}} \in \mathbb{E}$, where $\mathbb{E}$ is set of positive even integers photon-counting is not optimal but becomes increasingly close to optimal for increasing $N \geqslant 4 \in \mathbb{E}$ and Γ.

The optimality of photon counting applies to all optimal probes for all values of Γ whose mean energies $\bar{n} \in \mathbb{E}$, where $\mathbb{E}$ is the set of positive even integers. For such states, the optimal probes are all either odd ON states, for which the previous argument applies, or the pure, even Fock state after some value of Γ. When $\bar{n} \notin \mathbb{E}$, there exists a region $\Gamma \gtrsim 0.4$ in which the transition occurs between odd and even Fock state dominance. Before this, the optimal probes are odd ON states and the optimality of photon counting still applies, but after this, the optimal probe becomes a superposition of the lowest-lying even number states and photon counting is, unsurprisingly, sub-optimal. Despite this, restricting ourselves to photon counting in this regime still offers a quantum advantage compared to the coherent state benchmark. As $\Gamma \to 1$, the optimal probe tends to a superposition of the lowest-lying even number states, whose QFI across the entire

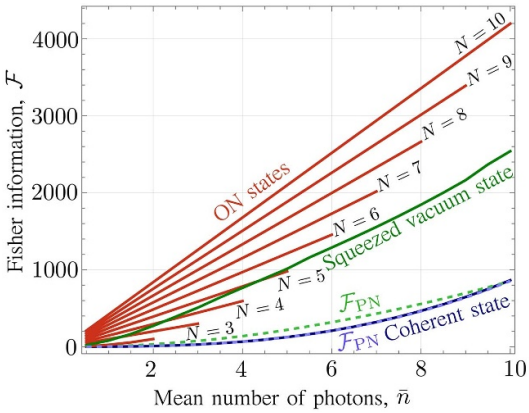

Figure 6. Scaling of QFI (solid), $\mathcal{F}_{\mathrm{Q}}$, and FI (dashed) due to photon number measurements, $\mathcal{F}_{\hat{n}}$, with the mean number of photons, $\bar{n}$, for $\Gamma = 0.01$. Results are shown for the coherent and squeezed vacuum states, as well as the ON state $|\mathrm{ON}\rangle = \sqrt{1-\bar{n}/N}|0\rangle + \sqrt{\bar{n}/N}|N\rangle$ which extends from different ON states, labeled with associated N-value, to the pure Fock state with $\bar{n} = N$.

region $\Gamma \gtrsim 0.4$ is somewhat comparable to the maximal ones found through optimisation. Correlations between these non-zero states provide additional contributions to the QFI which render photon counting sub-optimal here. However, in the large TPA limit where they are truly optimal, they become negligible and photon counting is very nearly optimal.

3.4. Scaling of FI with mean

The scaling of both the QFI, $\mathcal{F}_{\mathrm{Q}}$, and FI based on photon counting, $\mathcal{F}_{\mathrm{PN}}$, with the mean probe energy $\bar{n}$ for each of the quantum states considered is shown in figure 6 for $\Gamma = 0.01$. Here, we consider the ON state $|\mathrm{ON}\rangle = \sqrt{1-\bar{n}/N}|0\rangle + \sqrt{\bar{n}/N}|N\rangle$ (labelled by N) which extends, with increasing $\bar{n}$, from the ON state to the pure Fock state with $\bar{n}$ for a given N. For these states, when N is odd we have $\mathcal{F} = \mathcal{F}_{\mathrm{PN}}$, while when N is even, we have $\mathcal{F} \simeq \mathcal{F}_{\mathrm{PN}}$, with the difference becoming smaller for the larger N values. Known behaviours of coherent and squeezed vacuum states are also recovered. Meanwhile the ON/Fock states show an improvement in TPA parameter estimation over the squeezed vacuum state for some choice of N and there is always a quantum advantage compared to coherent states.

3.5. FI of photon counting with nonunity detection efficiency

We have demonstrated above that the maximised QFIs for TPA parameter estimation associated with our optimal probe states can almost always be saturated by photon counting. This is particularly true for the practical regime of small-to-intermediate scales of TPA strength. Nevertheless, there are typically inefficiencies associated with any practical measurement scheme that can potentially destroy any quantum advantage. In this section, we examine the robustness of the quantum advantage to single-photon losses downstream of the two-photon interaction. In particular, this includes the nonunity quantum efficiency of any realistic photon counting device.

Such inefficiencies can be included by modelling the detection process (characterised by a detection efficiency $\xi < 1$) as generating a conditional binomial distribution of PN followed by ideal photon counting. The actual probability of measuring n photons is then

$$p(n|\varepsilon) = \sum_{m \geqslant n} \binom{m}{m-n} \xi^m (1-\xi)^{m-n} p(m|\varepsilon), \tag{17}$$

where $p(m|\varepsilon)$ is the probability of measuring m photons in the light field immediately after interacting with the sample with TPA strength ε (and is calculated by solving equation (B1) in appendix B). The resulting FI, denoted $\mathcal{F}_{\mathrm{PN},\xi}$, is calculated directly by using the PN distribution in the definition equation (5).

Figure 7 plots the FI based on photon counting, as a function of photo-detection efficiency ξ, for squeezed vacuum, coherent, Fock and ON state probes of the form $\sqrt{1-\bar{n}/N}|0\rangle + \sqrt{\bar{n}}/N|N\rangle$. The mean PN is set to $\bar{n} = 2$ and, for the ON state, results are shown for $N = 5, 7$ and 9. The quantum advantage offered by ON states for TPA parameter estimation is robust across all scales of efficiency ξ and can be seen to increase with the value of N. The use of a pure Fock states $|\bar{n}\rangle$ maintains some quantum advantage for high efficiency $\xi \gtrsim 0.85$, depending on the value of $\bar{n}$, but soon lose any quantum advantage compared to coherent states for this given measurement set-up.

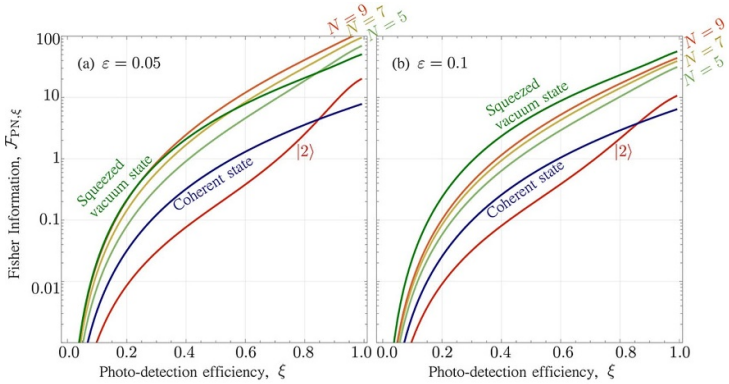

Figure 7. Scaling of the Fisher information (FI) $\mathcal{F}_{\mathrm{PN},\xi}$ of photon number measurements as a function of detection efficiency ξ. Results are shown for mean photon number $\bar{n} = 2$ with true TPA rates $\varepsilon = 0.05$ and 0.1. Results are shown for the Fock, coherent, squeezed vacuum and ON states, $|\mathrm{ON}\rangle = \sqrt{1-\bar{n}/N}|0\rangle + \sqrt{\bar{n}/N}|N\rangle$, where the associated N-value is labelled.

To obtain the results for the FI scaling with photo-detection efficiency depicted in figure 7, the true TPA rate has been set to values $\varepsilon = 0.05$ and 0.1 ($\simeq \Gamma$, in both cases). With practicality in mind, this value has been taken as, generally the larger, of typical reported measurement values based on experiments [25–27]. In the latter case, while the quantum advantage of ON states is robust, their optimality disappears, with the squeezed vacuum proving to be optimal in this regime. Slightly weaker TPA rates see the optimality of ON states return once more. Our expectation is that the quantum advantage and optimality observed with ON states will be further enhanced for smaller values of TPA rate and further still with increasing N.

4. Conclusion

We have determined that, for small to intermediate TPA rates, the optimal probe for TPA parameter estimation is the absorption-dependent ON state for a given, fixed mean. That is, a superposition of the vacuum and, for increasing absorbance, progressively decreasing-energy (odd) Fock states, weighted to satisfy the mean constraint. In the limit of large loss, the optimal probe reduces to the pure Fock state when $\bar{n} \in \mathbb{E}$, otherwise, a superposition of the lowest-lying even number states.

Our findings have identified a stark contrast between the QFI behaviours of even and odd Fock states beyond the limit of vanishing absorbance which explains the form of the optimal probe: the latter's QFI dominates in the intermediate regime while in the limit of infinite absorption, tends towards zero. In this region, the QFI of even number states diverge once more, akin to the squeezed vacuum and coherent states, providing further insight into the already-known limiting behaviours of Gaussian probes, namely the coherent and squeezed vacuum state, to which our results are compared.

Remarkably, when the optimal probe takes the form of an odd ON state or even Fock state, the optimal measurement is simple photon counting. In this case we also show that the quantum advantage of the FI under photon counting is robust to single-photon loss. Otherwise, in the limit of large TPA and for $\bar{n} \notin \mathbb{E}$, photon counting forms a very nearly optimal measurement.

Future research could extend this to uncover the effects of one-photon loss, as done in [24] for Gaussian states, arising from potential experimental inefficiencies to determine the practical capabilities of such schemes. Another direction would be the consideration of two-mode problems with ancilla entanglement [40] to determine whether additional quantum features can be exploited to further increase sensitivity.

Data availability statement

All data that support the findings of this study are included within the article (and any supplementary files).

Acknowledgments

A K, K-G L, and C L are supported by Institute for Information & communications Technology Planning & Evaluation (IITP) grant funded by the Korea government (MSIT) (RS-2023-00222863). A K and C L are also supported by the National Research Council of Science & Technology (NST) grant by the Korea government (MSIT) (No. CAP22052-000). R N is supported by the Singapore Ministry of Education Tier 2 Grant No.

T2EP50221-0014. A C acknowledges the Ministry of Education, Singapore and the National Research Foundation, Singapore and the NRF QEP Grant NRF2021-QEP2-02-P03.

Appendix A. Effect of TPA on arbitrary quantum states

Recall from the main text that our TPA model is given by

$$\frac{\mathrm{d}\hat{\rho}_t}{\mathrm{d}t} = \gamma \mathscr{L}\hat{\rho}_t \equiv \frac{\gamma}{2}\left(\hat{a}^2\,\hat{\rho}_t\,\hat{a}^{\dagger 2} - \frac{1}{2}\hat{\rho}_t\hat{a}^{\dagger 2}\hat{a}^2 - \frac{1}{2}\hat{a}^{\dagger 2}\hat{a}^2\,\hat{\rho}_t\right) . \tag{A1}$$

This has been solved exactly using different methods [34–38]. Here we provide a brief discussion of the solution provided by [38] in a more transparent notation. When parametrised in terms of $\varepsilon = \gamma\, t$, this gives an output state of the form

$$\hat{\rho}_\varepsilon = \sum_{l=0}^{\infty}\sum_{k=l}^{\infty} \frac{(-1)^l}{(k-l)!\,l!}\,\frac{\exp\left[-(\varepsilon/4)\,\mathscr{K}_l\right]}{\mathscr{J}_{k,l}}\,\hat{a}^{2k}\,\hat{\rho}_0\,\hat{a}^{\dagger 2k} , \tag{A2}$$

for any input state $\hat{\rho}_0$. The superoperators $\mathscr{K}_l$ and $\mathscr{J}_{k,l}$ are defined by

$$\mathscr{K}_l\hat{s} \equiv \left\{(\hat{n}+2l)\,(\hat{n}+2l-1)\,,\hat{s}\right\} , \tag{A3}$$

$$\mathscr{J}_{k,l}\hat{s} \equiv \prod_{\substack{m=0\\(m\neq l)}}^{k}\left\{2\hat{n}+2m+2l-1,\hat{s}\right\} , \tag{A4}$$

where $\{\hat{r},\hat{s}\} \equiv \hat{r}\hat{s}+\hat{s}\hat{r}$ for any $\hat{r}$ and $\hat{s}$. Note that $\mathscr{J}_{k,l}$ appears in the denominator of a superoperator fraction in equation (A2). This denotes a superoperator $\mathscr{J}_{k,l}^{-1}$ such that

$$\mathscr{J}_{k,l}^{-1}\,\mathscr{J}_{k,l} = \mathscr{J}_{k,l}\,\mathscr{J}_{k,l}^{-1} = \mathbb{1} , \quad \left[\mathscr{J}_{k,l}^{-1},\mathscr{K}_l\right] = 0 . \tag{A5}$$

It can be verified from equations (A3) and (A4) that such a $\mathscr{J}_{k,l}^{-1}$ always exists, and the superoperator fraction in equation (A2) is well defined (i.e. can be read without any ambiguity).

In practice, we find it convenient to rewrite equation (A2) in a slightly different way:

$$\begin{aligned}\hat{\rho}_\varepsilon &= \sum_{l=0}^{\infty}\sum_{k'=0}^{\infty} \frac{(-1)^l}{k'!\,l!}\,\frac{\exp\left[-(\varepsilon/4)\,\mathscr{K}_l\right]}{\mathscr{J}_{l+k',l}}\,\hat{a}^{2(l+k')}\,\hat{\rho}_0\,\hat{a}^{\dagger 2(l+k')}\\ &= \sum_{k=0}^{\infty}\sum_{l=0}^{k} \frac{(-1)^l}{(k-l)!\,l!}\,\frac{\exp\left[-(\varepsilon/4)\,\mathscr{K}_l\right]}{\mathscr{J}_{k,l}}\,\hat{a}^{2k}\,\hat{\rho}_0\,\hat{a}^{\dagger 2k}.\end{aligned} \tag{A6}$$

The first equality simply expresses the sum over k in equation (A2) as a sum over $k' \equiv k-l$. The second equality follows on first reordering the double sum in equation (A6), dropping the prime on the dummy index k', and then using the following identity for any summand $S_{k,l}$

$$\sum_{k=0}^{\infty}\sum_{l=0}^{\infty} S_{k,l} = \sum_{k=0}^{\infty}\sum_{l=0}^{k} S_{k-l,l} . \tag{A7}$$

The numerical results in the main text have been obtained with equation (A6) where necessary since it provides a straightforward way to reason about the quantum state's dynamics and carry out calculations. This final form limits us to considering only a single infinite sum, which can readily be limited by the input quantum state $\hat{\rho}_0$ in its Fock representation. Also, since the second summation is confined for each k, each term in k simply corresponds to the order of the TPA transition, i.e. for $k=1$ it refers to the transition $|n\rangle \to |n-2\rangle$. It is worth highlighting again that equation (A6) permits us to consider a much larger set of input states for the estimation of TPA rates than had been possible previously.

Appendix B. PN distribution and FI

The FI based on photon counting may be determined directly via the input PN distributions. In particular, one can make use of an alternative solution to the master equation which involves solving the system of differential equations given by

$$4\frac{\partial}{\partial\varepsilon}\langle n|\hat{\rho}_\varepsilon|n'\rangle = \left[(n+1)(n+2)(n'+1)(n'+2)\right]^{\frac{1}{2}}\langle n+2|\hat{\rho}_\varepsilon|n'+2\rangle - \frac{1}{2}\left[n(n-1)+n'(n'-1)\right]\langle n|\hat{\rho}_\varepsilon|n'\rangle . \tag{B1}$$

The FI with PN measurements can now be derived from equation (5) of the main text. The result is

$$\mathcal{F}_{\mathrm{PN}} = \sum_{n=0}^{\infty}\frac{\left[(n+1)(n+2)p(n+2|\varepsilon)-n(n-1)p(n|\varepsilon)\right]^2}{4p(n|\varepsilon)} \tag{B2}$$

where $p(n|\varepsilon)$ is the probability of measuring n photons in the state $\hat{\rho}_\varepsilon$, i.e.

$$p(n|\varepsilon) = \langle n|\hat{\rho}_\varepsilon|n\rangle = \mathrm{Tr}\left[|n\rangle\langle n|\hat{\rho}_\varepsilon\right] . \tag{B3}$$

Appendix C. Scaling of Fock state QFI in the limit of low TPA

To determine the scaling of the QFI/FI for Fock states with PN n, we first note that the QFI takes the simplified form for states diagonal in the Fock basis:

$$\mathcal{F}_{\mathrm{Q}} = \sum_{k=0}^{\infty}\langle k|\hat{L}_\varepsilon^2|k\rangle\langle k|\hat{\rho}_\varepsilon|k\rangle = \sum_{k=0}^{\infty}\frac{1}{h_k(n,\varepsilon)}\left[\frac{\partial}{\partial\varepsilon}h_k(n,\varepsilon)\right]^2 . \tag{C1}$$

We have defined the function $h_k(n,\varepsilon)$ to be

$$h_k(n,\varepsilon) \equiv \sum_{l=0}^{k}\frac{(-1)^l}{(k-l)!l!}\frac{n!}{(n-2k)!}F_{k,l}(n,\varepsilon) , \tag{C2}$$

where

$$F_{k,l}(n,\varepsilon) \equiv \frac{\exp\left[-\varepsilon(n-2k+2l)(n-2k+2l-1)/2\right]}{2\prod_{\substack{m=0\\(m\neq l)}}^{k}(2n-4k+2m+2l-1)} . \tag{C3}$$

The only possible contribution to the divergence of the Fock state's QFI, occurring when $h_k(n,\varepsilon)=0$, is from the term arising from a single case of TPA, i.e. $k=1$. The associated term in the summation for an arbitrary Fock state $\hat{\rho}_0 = |n\rangle\langle n|$ is given by

$$\frac{1}{h_1}\left(\frac{\partial h_1}{\partial\varepsilon}\right)^2 = \frac{n!}{8(2n-3)(n-2)!}\mathrm{e}^{-\left(6-n+n^2\right)\varepsilon/2}\frac{\left[\mathrm{e}^{3\varepsilon}(n-1)n-\mathrm{e}^{2n\varepsilon}\left(6-5n+n^2\right)\right]^2}{\mathrm{e}^{2n\varepsilon}-\mathrm{e}^{3\varepsilon}} . \tag{C4}$$

Computing a Laurent series for small ε, we then find that

$$\lim_{\varepsilon\to 0}\frac{1}{h_1}\left(\frac{\partial h_1}{\partial\varepsilon}\right)^2 = \frac{n(n-1)}{2\varepsilon} . \tag{C5}$$

Adapting the same procedure to determine ON state scaling in this same limit, first note that the single case of TPA occurs from the $|N\rangle$ state contribution which now has an extra weight $\bar{n}/N$ associated with it. Then, equation (C5) becomes

$$\lim_{\varepsilon\to 0}\frac{1}{h_1}\left(\frac{\partial h_1}{\partial\varepsilon}\right)^2 = \frac{\bar{n}}{N}\left[\frac{N(N-1)}{2\varepsilon}\right] = \frac{\bar{n}(N-1)}{2\varepsilon} . \tag{C6}$$

Taking into account the reparameterisation $\Gamma = 1-\exp(-\varepsilon)$ in the limit of $\Gamma\to 0$ for equations (C5) and (C6), it is straightforward to recover equations (13) and (14) of the main text, respectively.

Appendix D. Comparison between even and odd number state behaviours across TPA scales

D.1. Small-intermediate TPA

Consider as an initial probe the Fock state $|n\rangle$. After TPA evolution, the output state is diagonal in the PN basis and its QFI takes a simplified form of equation (C1), outlined in appendix C. Noting the form of equations (C2) and (C3), ultimately the QFI is a summation of individual terms over $k \in \left[0, \lfloor N/2 \rfloor\right]$, which indexes the order of the TPA transition, and $l \in [0, k]$.

Each of the k terms in the QFI, corresponding to the constituent number state $|n-2k\rangle$. Among these, the most dominant term in both k and l occurs when $k = l = 0$ and is proportional to $\binom{n}{2}^2 (1-\Gamma)^{\binom{n}{2}}$, where we have also taken into account the reparameterisation $\Gamma = 1 - \exp(-\varepsilon)$. Let us now consider the differing behaviours under $n \to 2n$ and $n \to 2n+1$, representing even and odd Fock state inputs (both with the same number k of QFI contributions), respectively. Then, this term becomes

$$\text{even}: \quad [n(2n-1)]^2 (1-\Gamma)^{n(2n-1)}, \tag{D1}$$

$$\text{odd}: \quad [n(2n+1)]^2 (1-\Gamma)^{n(2n+1)}. \tag{D2}$$

It is clear that odd number state contributions to the QFI initially have a larger value compared to those from even number states for small Γ, but decay much faster as Γ increases. This decay rate is larger still with higher number states, thus as Γ increases the value of optimal $N(\Gamma)$ decreases.

D.2. Large TPA

Consider now the behaviour seen in the limit of large loss as $\Gamma \to 1$ for even and odd Fock state QFI contributions. In particular, let us compare the QFI contribution associated with $k = 1$, $l = 1$ which, in terms of Γ, is proportional to

$$\text{even}: \quad (1-\Gamma)^{-2} (1-\Gamma)^{n(2n-1)} \to (1-\Gamma)^{-1}, \tag{D3}$$

$$\text{odd}: \quad (1-\Gamma)^{-2} (1-\Gamma)^{n(2n+1)} \to (1-\Gamma)^{1}, \tag{D4}$$

where the final limiting value is calculated for $n = 1$, referring to contributions from $|2\rangle$ and $|3\rangle$ states, respectively. Note that regardless of the initial state, all even and odd number states will, after TPA, end up with populations in these states and their QFI will have a contribution of this form. Considering what happens now with $\Gamma \to 1$, it is clear that an even number state's QFI will eventually diverge in this limit while an odd number state's QFI will become zero.

Appendix E. Phase insensitivity of the QFI

In this appendix, we justify the claim made in section 3.1.2 that the QFI for TPA loss is invariant to the direction of displacement for a coherent state probe, and to the squeezing direction for a squeezed state probe. Denote by $\hat{\rho}_0$ a coherent state with real-valued amplitude or a squeezed vacuum state with real squeezing parameter, as we assumed in section 3.1.2. The choice of a different displacement direction or squeezing axis corresponds to using a probe rotated by some angle ϕ, given by

$$\hat{\rho}(\phi) = \mathscr{P}_\phi \, \hat{\rho}_0 \,, \tag{E1}$$

where for any $\hat{s}$, the rotation (or phase-shift) superoperator is defined by

$$\mathscr{P}_\phi \, \hat{s} = \mathrm{e}^{-i\phi\hat{n}} \hat{s} \mathrm{e}^{i\phi\hat{n}} \,. \tag{E2}$$

It is straightfoward to see that

$$\mathscr{P}_\phi^{-1} \, \hat{s} = \mathrm{e}^{i\phi\hat{n}} \hat{s} \mathrm{e}^{-i\phi\hat{n}} \,, \tag{E3}$$

and, for any $\hat{r}$ and $\hat{s}$,

$$\mathscr{P}_\phi \, \hat{r}\hat{s} = (\mathscr{P}_\phi \, \hat{r})(\mathscr{P}_\phi \, \hat{s}) \,, \tag{E4}$$

$$\mathrm{Tr}\left[\hat{s} \, \mathscr{P}_\phi \, \hat{r}\right] = \mathrm{Tr}\left[\hat{r} \, \mathscr{P}_\phi^{-1} \, \hat{s}\right] \,. \tag{E5}$$

Let us denote the output state for an rotated input by

$$\hat{\rho}_\varepsilon(\phi) = \mathrm{e}^{\varepsilon\mathscr{L}}\,\hat{\rho}(\phi)\ . \tag{E6}$$

The output state for an unrotated input is then given by

$$\hat{\rho}_\varepsilon(0) = \mathrm{e}^{\varepsilon\mathscr{L}}\,\hat{\rho}(0) = \mathrm{e}^{\varepsilon\mathscr{L}}\,\hat{\rho}_0\ . \tag{E7}$$

Note that $\hat{\rho}_\varepsilon(0)$ is exactly what we have referred to as $\hat{\rho}_\varepsilon$ in the main text. The SLD for an output with a rotated input, i.e. $\hat{\rho}_\varepsilon(\phi)$, is then defined by an $\hat{L}_\varepsilon(\phi)$ such that

$$\frac{\partial}{\partial\varepsilon}\hat{\rho}_\varepsilon(\phi) = \frac{1}{2}\left[\hat{\rho}_\varepsilon(\phi)\,\hat{L}_\varepsilon(\phi) + \hat{L}_\varepsilon(\phi)\,\hat{\rho}_\varepsilon(\phi)\right]. \tag{E8}$$

Likewise, the SLD for an unrotated input state satisfies,

$$\frac{\mathrm{d}}{\mathrm{d}\varepsilon}\hat{\rho}_\varepsilon(0) = \frac{1}{2}\left[\hat{\rho}_\varepsilon(0)\,\hat{L}_\varepsilon(0) + \hat{L}_\varepsilon(0)\,\hat{\rho}_\varepsilon(0)\right], \tag{E9}$$

where $\hat{L}_\varepsilon(0)$ is precisely $\hat{L}_\varepsilon$ from the main text.

It was shown in [32] that

$$[\mathscr{P}_\phi, \mathscr{L}] = 0\ . \tag{E10}$$

Using equation (E10) we thus have

$$\begin{aligned}\hat{\rho}_\varepsilon(\phi) &= \mathrm{e}^{\varepsilon\mathscr{L}}\,\mathscr{P}_\phi\,\hat{\rho}(0)\\ &= \mathscr{P}_\phi\,\mathrm{e}^{\varepsilon\mathscr{L}}\,\hat{\rho}(0) = \mathscr{P}_\phi\,\hat{\rho}_\varepsilon(0)\ .\end{aligned} \tag{E11}$$

Now differentiating respect to ε, then using equations (E9) and (E4) gives

$$\begin{aligned}\frac{\partial}{\partial\varepsilon}\hat{\rho}_\varepsilon(\phi) &= \mathscr{P}_\phi\,\frac{\mathrm{d}}{\mathrm{d}\varepsilon}\hat{\rho}_\varepsilon(0)\\ &= \frac{1}{2}\left[\mathscr{P}_\phi\,\hat{\rho}_\varepsilon(0)\,\hat{L}_\varepsilon(0) + \mathscr{P}_\phi\,\hat{L}_\varepsilon(0)\,\hat{\rho}_\varepsilon(0)\right]\\ &= \frac{1}{2}\left\{\hat{\rho}_\varepsilon(\phi)\left[\mathscr{P}_\phi\hat{L}_\varepsilon(0)\right] + \left[\mathscr{P}_\phi\hat{L}_\varepsilon(0)\right]\hat{\rho}_\varepsilon(\phi)\right\}\ .\end{aligned} \tag{E12}$$

Equating equation (E12) to equation (E8) then implies that

$$\hat{L}_\varepsilon(\phi) = \mathscr{P}_\phi\,\hat{L}_\varepsilon(0)\ . \tag{E13}$$

Using equations (E4), (E5) and (E13), we can then show that $\mathcal{F}_\mathrm{Q}(\phi) \equiv \mathrm{Tr}\left[\hat{\rho}_\varepsilon(\phi)\hat{L}_\varepsilon^2(\phi)\right]$ is in fact independent of ϕ:

$$\begin{aligned}\mathcal{F}_\mathrm{Q}(\phi) &= \mathrm{Tr}\left[\hat{\rho}_\varepsilon(\phi)\left\{\mathscr{P}_\phi\,\hat{L}_\varepsilon(0)\right\}^2\right]\\ &= \mathrm{Tr}\left[\hat{\rho}_\varepsilon(\phi)\,\mathscr{P}_\phi\,\hat{L}_\varepsilon^2(0)\right]\\ &= \mathrm{Tr}\left[\hat{L}_\varepsilon^2(0)\,\mathscr{P}_\phi^{-1}\,\mathscr{P}_\phi\,\hat{\rho}_\varepsilon(0)\right] = \mathcal{F}_\mathrm{Q}(0)\ .\end{aligned} \tag{E14}$$

This completes our proof that no loss of generality is incurred by choosing a real-valued amplitude for $\hat{\rho}_0$ if it is a coherent state, or a real-valued squeezing parameter if it is a squeezed state.

ORCID iDs

Athena Karsa https://orcid.org/0000-0001-9096-8311
Ranjith Nair https://orcid.org/0000-0002-0186-4279
Changhyoup Lee https://orcid.org/0000-0002-1401-4230

References

[1] Giovannetti V, Lloyd S and Maccone L 2011 Advances in quantum metrology *Nat. Photon.* **5** 222–9
[2] Polino E, Valeri M, Spagnolo N and Sciarrino F 2020 Photonic quantum metrology *AVS Quantum Sci.* **2** 024703
[3] Genovese M 2016 Real applications of quantum imaging *J. Opt.* **18** 073002
[4] Mukamel S *et al* 2020 Roadmap on quantum light spectroscopy *J. Phys. B: At. Mol. Opt. Phys.* **53** 072002
[5] Klyshko D N 1982 Transverse photon bunching and two-photon processes in the field of parametrically scattered light *Sov. Phys. - JTEP* **56** 753
[6] Gea-Banacloche J 1989 Two-photon absorption of nonclassical light *Phys. Rev. Lett.* **62** 1603
[7] Javanainen J and Gould P L 1990 Linear intensity dependence of a two-photon transition rate *Phys. Rev.* A **41** 5088
[8] Georgiades N P, Polzik E S, Edamatsu K, Kimble H J and Parkins A S 1995 Nonclassical excitation for atoms in a squeezed vacuum *Phys. Rev. Lett.* **75** 3426
[9] Georgiades N P, Polzik E S and Kimble H J 1997 Atoms as nonlinear mixers for detection of quantum correlations at ultrahigh frequencies *Phys. Rev.* A **55** R1605
[10] Dayan B, Pe'er A, Friesem A A and Silberberg Y 2004 Two photon absorption and coherent control with broadband down-converted light *Phys. Rev. Lett.* **93** 023005
[11] Dorfman K E, Schlawin F and Mukamel S 2016 Nonlinear optical signals and spectroscopy with quantum light *Rev. Mod. Phys.* **88** 045008
[12] Schlawin F 2017 Entangled photon spectroscopy *J. Phys. B: At. Mol. Opt. Phys.* **50** 203001
[13] Schlawin F, Dorfman K E and Mukamel S 2018 Entangled two-photon absorption spectroscopy *Acc. Chem. Res.* **51** 2207
[14] Gilaberte Basset M, Setzpfandt F, Steinlechner F, Beckert E, Pertsch T and Gräfe M 2019 Perspectives for applications of quantum imaging *Laser Photon. Rev.* **13** 1900097
[15] Ma Y-Z and Doughty B 2021 Nonlinear optical microscopy with ultralow quantum light *J. Phys. Chem.* A **125** 8765
[16] Eshun A, Varnavski O, Villabona-Monsalve J P, Burdick R K and Goodson T III 2022 Entangled photon spectroscopy *Acc. Chem. Res.* **55** 991
[17] Pirandola S, Bardhan B R, Gehring T, Weedbrook C and Lloyd S 2018 Advances in photonic quantum sensing *Nat. Photon.* **12** 724–33
[18] Karsa A, Spedalieri G, Zhuang Q and Pirandola S 2020 Quantum illumination with a generic Gaussian source *Phys. Rev. Res.* **2** 023414
[19] Monras A and Paris M G A 2007 Optimal quantum estimation of loss in bosonic channels *Phys. Rev. Lett.* **98** 160401
[20] Adesso G, Dell'Anno F, De Siena S, Illuminati F and Souza L A M 2009 Optimal estimation of losses at the ultimate quantum limit with non-Gaussian states *Phys. Rev.* A **79** 040305
[21] Braunstein S L, Caves C M and Milburn G J 1996 Generalized uncertainty relations: theory, examples and Lorentz invariance *Ann. Phys., NY* **247** 135–73
[22] Maccone L 2006 Information-disturbance tradeoff in quantum measurements *Phys. Rev.* A **73** 042307
[23] Muñoz C S, Frascella G and Schlawin F 2021 Quantum metrology of two-photon absorption *Phys. Rev. Res.* **3** 033250
[24] Panahiyan S, Muñoz C S, Chekhova M V and Schlawin F 2022 Two-photon-absorption measurements in the presence of single-photon losses *Phys. Rev.* A **106** 043706
[25] Tabakaev D, Montagnese M, Haack G, Bonacina L, Wolf J-P, Zbinden H and Thew R T 2021 Energy-time-entangled two-photon molecular absorption *Phys. Rev.* A **103** 3
[26] Villabona-Monsalve J P, Varnavski O, Palfey B A and Goodson T III 2018 Two-photon excitation of flavins and flavoproteins with classical and quantum light *J. Am. Chem. Soc.* **140** 44
[27] Villabona-Monsalve J P, Burdick R K and Goodson T III 2020 Measurements of entangled two-photon absorption in organic molecules with CW-pumped type-I spontaneous parametric down-conversion *J. Phys. Chem.* C **124** 44
[28] Wiseman H M and Milburn G J 2010 *Quantum Measurement and Control* (Cambridge University Press)
[29] Helstrom C W 1967 Minimum mean-squared error of estimates in quantum statistics *Phys. Lett.* A **25** 101
[30] Braunstein S L and Caves C M 1994 Statistical distance and the geometry of quantum states *Phys. Rev. Lett.* **72** 3439
[31] Lambropoulos P 1967 Quantum statistics of a two-photon quantum amplifier *Phys. Rev.* **156** 286
[32] Chia A, Hajdušek M, Nair R, Fazio R, Kwek L C and Vedral V 2020 Phase-preserving linear amplifiers not simulable by the parametric amplifier *Phys. Rev. Lett.* **125** 163603 (see supplementary material)
[33] Chia A, Mok W-K, Noh C and Kwek L C 2023 Quantum pure noise-induced transitions: a truly nonclassical limit cycle sensitive to number parity *SciPost Phys.* **15** 121
[34] Simaan H D and Loudon R 1975 Quantum statistics of double-beam two-photon absorption *J. Phys. A: Math. Gen.* **8** 1140
[35] Simaan H D and Loudon R 1975 Quantum statistics of single-beam two-photon absorption *J. Phys. A: Math. Gen.* **8** 539
[36] Simaan H D and Loudon R 1978 Off-diagonal density matrix for single-beam two-photon absorbed light *J. Phys. A: Math. Gen.* **11** 435
[37] Gilles L and Knight P L 1993 Two-photon absorption and nonclassical states of light *Phys. Rev.* A **48** 1582
[38] Klimov A B and Romero J L 2003 An algebraic solution of Lindblad-type master equations *J. Opt. B: Quantum Semiclass. Opt.* **5** S316
[39] Toklu N E, Atkinson T, Micka V, Liskowski P and Srivastava R K 2023 EvoTorch: scalable evolutionary computation in Python (arXiv:2302.12600)
[40] Nair R and Gu M 2023 Quantum sensing of phase-covariant optical channels (arXiv:2306.15256)